High-speed three-dimensional shape measurement using geometry-constraint-based number-theoretical phase unwrapping

Wei Yin [a,b,c], Chao Zuo [a,b,c,*], Shijie Feng [a,b,c], Tianyang Tao [a,b,c], Yan Hu [a,b,c], Lei Huang [d], Jiawei Ma [a], Qian Chen [a,b]

[a] *School of Electronic and Optical Engineering, Nanjing University of Science and Technology, No. 200 Xiaolingwei Street, Nanjing, Jiangsu Province 210094, China*
[b] *Jiangsu Key Laboratory of Spectral Imaging & Intelligent Sense, Nanjing University of Science and Technology, Nanjing, Jiangsu Province 210094, China*
[c] *Smart Computational Imaging (SCI) Laboratory, Nanjing University of Science and Technology, Nanjing, Jiangsu Province 210094, China*
[d] *Brookhaven National Laboratory, NSLS II 50 Rutherford Drive, Upton, New York 11973-5000, United States*

ARTICLE INFO

ABSTRACT

In this paper, we propose a high-speed three-dimensional (3-D) shape measurement technique for dynamic scenes using geometry-constraint-based number-theoretical phase unwrapping. As a classical algorithm for temporal phase unwrapping (TPU), the number-theoretical approach is suitable for the binary defocusing fringe projection system since it can retrieve an absolute phase without using low-frequency fringe patterns. However, the conventional number-theoretical TPU approach cannot provide sufficient stability to unwrap a high-frequency phase since it requires the two fringe frequencies to be coprime within the global range of the projector coordinate. In contrast, using low-frequency fringe patterns tends to make phase unwrapping more reliable, but at the expense of the measurement precision. By introducing depth constraint into the traditional number-theoretical TPU, we only need to eliminate the phase ambiguity of each pixel within a small period range defined by the depth range, which means that our method just requires the two fringe frequencies to be coprime within the local period range instead of the conventional global range. Due to the reduction of fringe order candidates and the unambiguous phase range, the reliability of phase unwrapping can be significantly improved compared with the traditional number-theoretical TPU approach even when high-frequency fringe patterns are used. The proposed method has been successfully implemented on a high-frame-rate fringe projection system, achieving high-precision, robust, and absolute 3-D shape measurement at 3333 frames per second.

1. Introduction

Three-dimensional (3-D) shape measurement plays an increasingly important role in various fields such as machine design, medical science, entertainment, and so on. Among all the methods, fringe projection profilometry (FPP) is one of the high-performance techniques due to its accuracy and high efficiency. With the rapid development of the high-speed camera and high-speed digital light processing (DLP) projection technique, three-dimensional shape measurement of transient scenes such as high-speed motion and rapid deformation has attracted widespread attention [1–6]. According to the phase retrieval technique used for extracting the depth information of the measured surface, mainstream FPP approaches can be classified into two categories: Phase-shifting profilometry (PSP) [7,8] and Fourier transform profilometry (FTP) [9,10]. FTP is highly suited for dynamic 3D acquisition, which can obtain the phase map using one fringe pattern. But this method suffers from the spectrum overlapping, which limits its measurement

quality and makes it unable to recover the fine details of complex surfaces. In addition, instead of Fourier transform, the windowed Fourier transform (WFT) [11] and the wavelet transform (WT) [12] can also be used to achieve higher phase measurement accuracy from a single high-frequency fringe pattern. Compared with FTP, PSP is more used widely in FPP because it is more robust and can achieve pixel-wise phase measurement with higher resolution and accuracy. However, PSP generally requires more time to acquire the multiple fringe patterns to reconstruct the 3D shape of the object. Moreover, both methods adopt arctangent function and lead to the wrapped phase map with 2π phase jumps. Therefore, it is necessary to perform phase unwrapping to eliminate the phase ambiguity and convert the wrapped phase to the absolute phase [13,14].

Dozens of phase unwrapping approaches have been proposed and can be divided into two categories: spatial phase unwrapping [13] and temporal phase unwrapping (TPU) [14–17]. Spatial phase unwrapping refers to a class of methods for phase unwrapping using the relationship between the phase information of the spatial neighboring pixels

---

[13,18–21]. They are generally applied to recover a continuous phase map from a wrapped one, yet it cannot solve the ambiguity when multiple isolated objects or abrupt depth changes are present. In order to overcome the deficiencies in spatial phase unwrapping algorithm, TPU approaches have been developed to unwrap a more general phase map which may contain large discontinuities and separations. Typical temporal phase unwrapping algorithms can be classified as either gray-code approaches [15] or multi-frequency approaches [14]. In gray-code approaches, a set of binary gray-code patterns are sequentially projected over time for encoding the fringe order information, so N gray-code patterns can theoretically assist to unwrap the wrapped phase with 2^N-period. Consequently, it needs more additional gray-code patterns to eliminate the phase ambiguities of fringe patterns with high-frequency, which is not suitable for high-speed 3D measurement. To address the disadvantages of gray-code approaches, a phase-coding method is proposed for absolute phase retrieval by embedding the N-bit stair phase (2^N level) into the phase component of phase-shifting fringe patterns [16], and the stairs can be used to determine the fringe order for phase unwrapping. However, due to the defocusing effect of the projector and the random noise of the system, some post-processing algorithms must be performed to effectively reduce the errors on the unwrapped phase map [17]. Besides, multi-frequency approaches unwrap the wrapped phase map with the aid of additional wrapped phase maps with different fringe periods. Since the minimum number of patterns required in standard phase-shifting algorithm is three, if we implement multi-frequency approaches based on standard PSP algorithms, at least six patterns (two separate 3-step phase-shifting patterns) should be used for obtaining two wrapped phases. Obviously, the increased number of required patterns is undesirable for high-speed measurement applications, where it is preferable to minimize the acquisition time to reduce the potential motion-induced artifacts.

In dynamic 3-D shape measurement [22–30], increasing the speed of the hardware (projector and camera) is also essential to improve the measurement quality and reduce the motion artifacts. Because the digital mirror device, as the key component of the DLP projector is a binary digital device (can be either 'on' or 'off'), the binary defocusing technique [31,32] is widely applied to the digital fringe projection system to increase the projection rate up to tens of kilo-Hz [25,29]. By properly optimizing the binary patterns, quasi-sinusoidal fringe patterns can be created by slightly defocusing the projector lens. However, due to the limited defocusing level of the projector lens, it is much more difficult to generate desired low-frequency fringe patterns than high-frequency ones [33]. Therefore the multi-wavelength TPU approach [34–36] and the number-theoretical TPU approach [37–40] are usually used in the binary defocusing projection system since it can avoid the acquisition of low-frequency fringe patterns. Furthermore, compared with the multi-wavelength TPU approach, the number-theoretical TPU method provide better unwrapping reliability and noise tolerance [14]. Zuo et al. [22] proposed a high-speed 3-D measurement technique using bi-frequency tripolar pulse-width-modulation (TPWM) fringe projection and the number-theoretical approach. However, to ensure the stability of phase unwrapping, the fringe patterns used are usually designed with a relatively low frequency, e.g., 20 stripes, which results in low measurement precision.

Besides TPU, geometry-constraint-based approaches are also very efficient to solve the phase ambiguity problem for measuring complex surfaces. Geometry constraint has been widely used in stereo vision because it can help binocular cameras find the corresponding points in different perspectives more effectively [41]. For a FPP system, geometry constraint requires that the correspondences between the camera and the projector are only selected along the polar line, which reduces the search area and improves the efficiency of phase unwrapping [23,27,42–47]. If the pre-knowledge about the measurement range of the system can be obtained, depth constraint can be applied to further excluding false candidates located outside the measurement volume and enhancing the stability of phase unwrapping. Based on this idea, An et al. presented a

method to unwrap phase pixel by pixel by solely using geometric constraints of the structured light system without requiring additional image acquisition or another camera [45]. Based on geometric constraint, an artificial absolute phase map Φ_{min} is created as a reference to unwrap the wrapped phase pixel-by-pixel. The wrapped phase with high-frequency can be unwrapped directly in the narrow depth range using this method. Inspired by An's method, Hyun et al. used more than one period of the low-frequency phase or stair patterns to unwrap or encode high-frequency fringe orders by introducing the minimum phase map Φ_{min} into two-frequency method and phase-coding approaches [17,48]. But, in order to ensure the stability of phase unwrapping, the period of the low-frequency phase or stair patterns can only be increased to 2 or 3 times on account of the defocusing effect of the projector and the random noise of the system, so the period of high-frequency fringe is generally around 30 pixels which limits the quality of 3D measurement. In the binary defocusing projection system, the narrower fringe patterns are commonly used to achieve high-quality measurement. To achieve high-precision measurement, Tao et al. presented a multi-view system based on geometry constraint to increase the fringe density so that the measurement precision can be improved greatly in real-time 3-D shape measurement [27]. Based on depth constraint, the low-frequency (10-period) phase map is unwrapped directly since it is "absolute" in the local range. The obtained absolute phase map can be used to unwrap the high-frequency one through multi-frequency phase unwrapping. However, as mentioned above, the number-theoretical TPU approach [37,38,40] is more suitable for high-speed 3-D shape measurement based on binary defocusing projection because it can avoid the acquisition of low-frequency fringe patterns. However, in conventional number-theoretical TPU, two fringe frequencies should be co-prime within the global range of the projector coordinate. How to incorporate the geometry constraint into number-theoretical TPU to improve the phase unwrapping stability and measurement precision is still an important problem that needs to be addressed.

To this end, this paper presents a high-speed three-dimensional shape measurement approach using geometry-constraint-based number-theoretical phase unwrapping. Due to the limited depth of field of the camera (to maximize the image brightness, the camera lens usually has a large aperture) as well as the limited depth measurement range of a slightly defocused projector (the object must be properly placed in a small region such that the binary pattern becomes good-quality sinusoidal), it is reasonable and necessary that number-theoretical TPU and the binary defocusing technique should be used in combination with the depth constraint approaches. Owing to the advantage of depth constraint, we only need to eliminate the phase ambiguity within a small period range defined by the depth range, which means that our method just requires the two fringe frequencies to be coprime within the local period range instead of the conventional global range. The accuracy of phase unwrapping is higher in the local period range due to containing fewer period ambiguities. As a result, we can realize reliable phase unwrapping of higher frequency fringes compared with the traditional number-theoretical TPU. Experiments demonstrate the capability of the method to achieve robust 3-D shape measurement for complex surfaces and spatially isolated objects. We also implement the proposed approach on a high-frame-rate fringe projection system, achieving high-precision, robust, and absolute 3-D shape measurement at 3333 frames per second.

In particular, it should be noted that we are not the first to apply depth constraint for phase unwrapping. Recently, some methods have been developed by combining TPU approaches and depth constraint successfully, but it just simply increase the period of the low-frequency fringe or stair patterns for phase unwrapping with high-frequency [17,27,48]. However, as it is widely known, the number-theoretical phase unwrapping method provides more complicated schemes for fringe frequency selection. In this work, we first present the use of depth constraint to achieve number-theoretical phase unwrapping with high-frequency fringes. By deriving a rigorous mathematical model to quantify the phase unwrapping error in the numerical theoretical TPU under

depth constraint, our method can provide a guideline for the selection strategy of the optimal bi-frequency scheme. The performance of our method is quantified and demonstrated using a standard ceramic sphere with a radius of 25.4 mm, which leads to a speed of 3333 frames per second (fps) with 51-period fringe patterns for fast, dense, and accurate 3-D measurement with a depth precision of 54 μm.

The remainder of this paper is organized as follows. In Section 2, the principle of the bi-frequency phase-shifting algorithm is firstly recalled, which is used to obtain two high-frequency wrapped phase maps. Then, the number-theoretical TPU approach based on depth constraint is proposed to unwrap the two high-frequency phase maps. Moreover, the performance of the proposed method in terms of noise resistance is discussed in detail. And the selection strategy of the optimal bi-frequency scheme is proposed to improve the stability of the absolute phase recovery under the condition of noise. Simulations and experimental verifications are presented in Sections 3 and dummyTXdummy- 4. Finally, conclusions are drawn in Section 5.

2. Principle

2.1. Bi-frequency phase-shifting algorithm

The N-step phase-shifting algorithm is widely used in FPP because it is quite robust to ambient illumination and varying surface properties [8,49–51]. In high-speed 3-D shape measurement, using the minimum number of fringe images is desirable for reducing the measurement time, so the three-step phase-shifting algorithm is widely used for decreasing the sensitivity to the object motion. However, this algorithm is still sensitive to different types of errors, such as system nonlinearity. In our method, the four-step phase-shifting algorithm is used for its relatively high measurement accuracy and good error tolerance. The standard four-step phase-shifting fringe patterns with shift offset of $\pi/2$ can be described as

$$I_n(x, y) = A(x, y) + B(x, y)\cos(\Phi_H(x, y) - n\pi/2) \tag{1}$$

where I_n is the fringe image captured by the camera, and n represents the phase-shifting index $n = 0, 1, 2, 3$. $A(x, y)$ is the average intensity, $B(x, y)$ is the intensity modulation, and $\Phi_H(x, y)$ is the phase information of the measured object. According to the least-squares algorithm, the wrapped phase map $\phi_H(x, y)$ can be obtained.

$$\phi_H(x, y) = \tan^{-1}\frac{\sum_{n=0}^{3} I_n(x, y)\sin(n\pi/2)}{\sum_{n=0}^{3} I_n(x, y)\cos(n\pi/2)} \tag{2}$$

Since the output domain of the $\tan^{-1}$ function ranges from $-\pi$ to π, the phase obtained by Eq. (2) will have 2π discontinuities. In TPU algorithms, we need an additional phase with different frequency as an assistance to obtain the absolute phase [14]. To reduce the total number of projection patterns, we use the bi-frequency phase-shifting algorithm [8,22] and project only two additional fringe patterns, which are represented as

$$I_{L1}(x, y) = A(x, y) + B(x, y)\sin\Phi_L(x, y)$$
$$I_{L2}(x, y) = A(x, y) + B(x, y)\cos\Phi_L(x, y) \tag{3}$$

In bi-frequency phase-shifting algorithm, the average intensity $A(x, y)$ is assumed to be the same in I_n, I_{L1}, and I_{L2} during a short time, which can be derived from Eq. (1):

$$A(x, y) = \frac{1}{4}\sum_{n=0}^{3} I_n(x, y) \tag{4}$$

Subsequently, the wrapped phase map $\phi_L(x, y)$ of second fringe pattern can be calculated

$$\phi_L(x, y) = \tan^{-1}\frac{I_{L1}(x, y) - A(x, y)}{I_{L2}(x, y) - A(x, y)} \tag{5}$$

Then, we obtain two wrapped phases $\phi_H(x, y)$ and $\phi_L(x, y)$ of different frequencies.
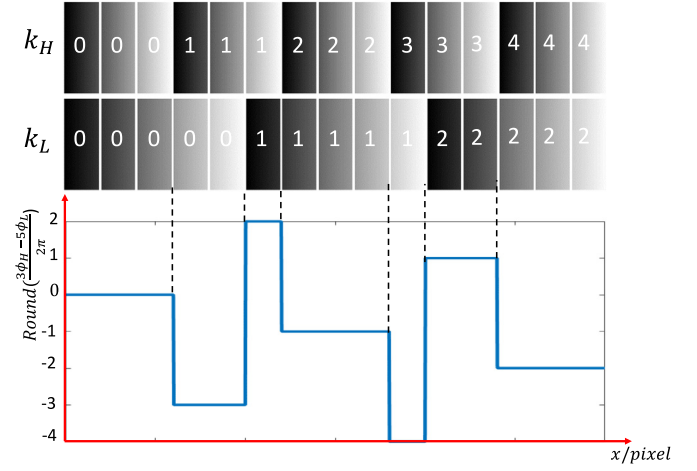
Fig. 1. The traditional number-theoretical approach for two wavelengths of 3 and 5 pixels. We can find a unique combination of $k_H(x, y)$ and $k_L(x, y)$ satisfying Eq. (10) for any valid pixel.

2.2. The number-theoretical approach based on depth constraint

The binary defocusing technique [31] is applied to our system to greatly improve the projection rate, but it cannot generate a high-quality low-frequency fringe pattern. Based on this technique, $\Phi_L(x, y)$ is not the phase map of unit-frequency but high-frequency. So the number-theoretical method is suitable for the binary defocusing projection system since it can retrieve an absolute phase without using low-frequency fringe patterns. In the traditional number-theoretical approach, the absolute phase map can be obtained by the following formula:

$$\Phi_H(x, y) = \phi_H(x, y) + 2\pi k_H(x, y)$$
$$\Phi_L(x, y) = \phi_L(x, y) + 2\pi k_L(x, y) \tag{6}$$

and the relationship is attached intrinsically:

$$\Phi_H(x, y) = \frac{\lambda_L}{\lambda_H}\Phi_L(x, y) \tag{7}$$

Typically, λ_H and λ_L stand for the wavelengths of the patterns I_n and I_{L1} to I_{L2}, respectively. $k_H(x, y)$ and $k_L(x, y)$ in Eq. (6) are the fringe orders to represent phase jumps. The core challenge for the absolute phase map recovery is to calculate $k_H(x, y)$ and $k_L(x, y)$ for each pixel in the phase map quickly and accurately. From the principle of number-theoretical approach [22], it can correctly unwrap the phase up to the value in the absolute phase which equals to $LCM(\lambda_H, \lambda_L)$. $LCM()$ stands for a function whose output is the least common multiple for input parameters. Eq. (7) can be rewritten as

$$p_L\Phi_H(x, y) = p_H\Phi_L(x, y) \tag{8}$$

where $p_H = LCM(\lambda_H, \lambda_L)/\lambda_H$, $p_L = LCM(\lambda_H, \lambda_L)/\lambda_L$. p_H and p_L represent the total number of fringes for the corresponding wavelength within the unambiguous range $LCM(\lambda_H, \lambda_L)$. Combining Eqs. (6) and (8) yields

$$\frac{p_L\phi_H(x, y) - p_H\phi_L(x, y)}{2\pi} = p_H k_L(x, y) - p_L k_H(x, y) \tag{9}$$

In practice, p_L, p_H, $k_L(x, y)$ and $k_H(x, y)$ are integers, where $k_i(x, y)$ ranges from 0 to $(p_i - 1)$ $(i = L, H)$. Generally, Eq. (9) can be adapted as

$$Round(\frac{p_L\phi_H(x, y) - p_H\phi_L(x, y)}{2\pi}) = p_H k_L(x, y) - p_L k_H(x, y) \tag{10}$$

where $Round()$ is a rounding function. Within the unambiguous range $LCM(\lambda_H, \lambda_L)$, we can only find a unique combination of $k_H(x, y)$ and $k_L(x, y)$ satisfying Eq. (10) for any valid pixel. As shown in Fig. 1, $\Phi_H(x, y)$ and $\Phi_L(x, y)$ can be obtained while $k_L(x, y)$ and $k_H(x, y)$ are
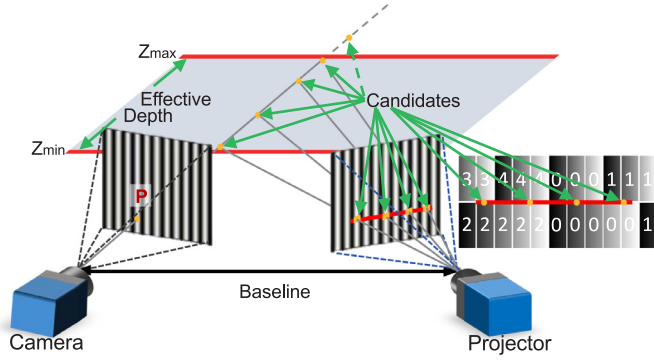
Fig. 2. Illustration of an arbitrary point p in the camera and its corresponding points in 3-D space and the projector using the number-theoretical approach based on depth constraint.

achieved correctly. Due to the limitations of the traditional number-theoretical approach, the phase only can be carried out unambiguous unwrapping within the range $LCM(\lambda_H, \lambda_L)$. Subsequently, it is necessary that the wavelengths of fringes should be selected suitably to satisfy $W < LCM(\lambda_H, \lambda_L)$ (W is the horizontal resolution of fringe patterns). Therefore, λ_H and λ_L are large in general, it i.e. the frequencies are low, which limits the accuracy of 3-D shape measurement.

In order to overcome the problems mentioned above, depth constraint is introduced into the traditional number-theoretical approach. Depth constraint has been widely used in stereo vision because it can help binocular cameras find the corresponding points in different perspectives more effectively. In FPP, we usually regard the projector as a reverse camera, so the principle of depth constraint can be applied to establish a point-to-point mapping relationship between the camera and the projector [27]. Once the measurement system is calibrated, the absolute phase map and depth information in the real world can be derived from the following formula [52]

$$Z(x, y) = f(x_p(x, y)),$$
$$x_p(x, y) = \frac{\Phi_H(x, y)}{2\pi N_H} W, \tag{11}$$

where $x_p(x, y)$ is the coordinate along the horizontal direction of projector, N_H is the number of periods of the sinusoidal fringes, and $Z(x, y)$ is the height in 3-D space. With the assistance of Eq. (11), the phase $\Phi_H(x, y)$ can lead directly to the 3-D position using calibration parameters between the camera and the projector. In general, due to the constraint of the depth of field of the camera and the limitation of the area at the slight defocusing state of the projector, it is to assume appropriately that the optimal depth range of measurement is $[Z_{\min}, Z_{\max}]$ in this system. According to Eq. (11), the range of each pixel of the camera corresponds to the projector is $[x_1(x, y), x_2(x, y)]$. For simplicity, $[x_1(x, y), x_2(x, y)]$ can be derived as

$$L = max[x_2(x, y) - x_1(x, y)] \tag{12}$$

If a suitable depth range is set such that $L < LCM(\lambda_H, \lambda_L)$, the operation of global phase unwrapping can be independent from the limit of $W < LCM(\lambda_H, \lambda_L)$. To illustrate the proposed method, the schematic diagram is shown in Fig. 2. Applying depth constraint, we only need to eliminate the period ambiguities of the arbitrary pixel within a pixel-variant local period range. In this way, the requirement of the traditional number-theoretical method for the coprime of two fringe frequencies can be adjusted from global range to local range. Obviously, the improved number-theoretical approach can further reduce the wavelengths of the bi-frequency scheme and realize phase unwrapping of higher frequency fringes which can yield more accurate and dense 3-D reconstruction results.

2.3. The selection strategy of the optimal bi-frequency scheme

In the subsection above, we have explained the basic principles and limitations of the number-theoretical approach as well as the corresponding improvement using depth constraint. However, the effect of noise, a notable factor in practice, is not considered. Consequently, how to improve the stability of the absolute phase recovery under the effect of noise is the key task in most TPU algorithms. Namely, in accordance with the improved number-theoretical approach, how to decide the optimal frequencies of the bi-frequency scheme is our main concern. Ding et al. [39] have proposed a selection method in absolute phase maps recovery with two frequency projection fringes, which indicates that error will occur in determining the fringe orders if the maximal phase error is larger than $\pi/(p_1 + p_2)$. Referring to this result, we propose a fringe selection method combined with depth constraint to find the maximal phase error according to Eq. (10). For simplicity, Eq. (10) is rewritten as

$$\begin{cases} Round(F(x, y)) = Stairs(x, y) \\ F(x, y) = (\dfrac{p_L \phi_H(x, y) - p_H \phi_L(x, y)}{2\pi}) \\ Stairs(x, y) = p_H k_L(x, y) - p_L k_H(x, y) \end{cases} \tag{13}$$

Assuming phase errors in the wrapped phase maps $\phi_H(x, y)$ and $\phi_L(x, y)$ are $\Delta\phi_H(x, y)$ and $\Delta\phi_L(x, y)$ respectively, we have:

$$\Delta F(x, y) = (\frac{p_L \Delta\phi_H(x, y) - p_H \Delta\phi_L(x, y)}{2\pi}) \tag{14}$$

Let $\Delta\phi_{\max} = \max(|\Delta\phi_H(x, y)|, |\Delta\phi_L(x, y)|)$, from Eq. (14) we can find the upper bound of $\Delta F(x, y)$:

$$\begin{aligned} \Delta F_{max}(x, y) &= |\frac{p_L \Delta\phi_H(x, y) - p_H \Delta\phi_L(x, y)}{2\pi}| \\ &= \Delta\phi_{max} \frac{p_L + p_H}{2\pi} \end{aligned} \tag{15}$$

To avoid errors in determining the fringe orders, from Eqs. (13) and (15) we have:

$$\Delta F_{max}(x, y) = \Delta\phi_{max} \frac{p_L + p_H}{2\pi} < 0.5N \tag{16}$$

Subsequently, we can confirm the boundary of $\Delta\phi_{\max}$:

$$0 \le \Delta\phi_{max} < \frac{\pi N}{p_L + p_H} \tag{17}$$

Notably, N is the minimum gap of $Stairs(x, y)$ within the unambiguous range, and Eq. (17) defines the range of $\Delta\phi_{\max}$ where the absolute phase can be correctly recovered. Otherwise, error will occur in determining the exact $k_L(x, y)$ and $k_H(x, y)$. Due to the fact that the unambiguous range is also the global range using the traditional number-theoretical approach, the default value of N is 1. However, with different depth constraints, the value of N varies in different local range. And our essential challenge is to find the corresponding N in the given local range defined by the depth constraint to maximize the value of $\pi N/(p_L + p_H)$.

Subsequently, a simple and effective selection strategy for maximizing $\pi N/(p_L + p_H)$ is proposed in our work. To clearly indicate the implementation procedure of the selection strategy, a flowchart is plotted as shown in Fig. 3. With the assistance of the example, the detail of the strategy is described as follows:

Step 1 Draw the distribution of *Stairs(x, y)*: Combining the maximal range of depth constraint in the projector space L, the horizontal resolution of the projection pattern W, and the wavelength of the bi-frequency scheme (λ_H, λ_L), the distribution of $Stairs(x, y)$ can be drawn according to Eq. (13), as shown in Fig. 4.

Step 2 Find the target point: The first point is considered as the reference point O, the value of which is 0 for any $Stairs(x, y)$. For the full field (W), the candidate points are the points that have the smallest difference of value with the reference O, and the one closest to the reference point O is selected, as the point A in Fig. 4.
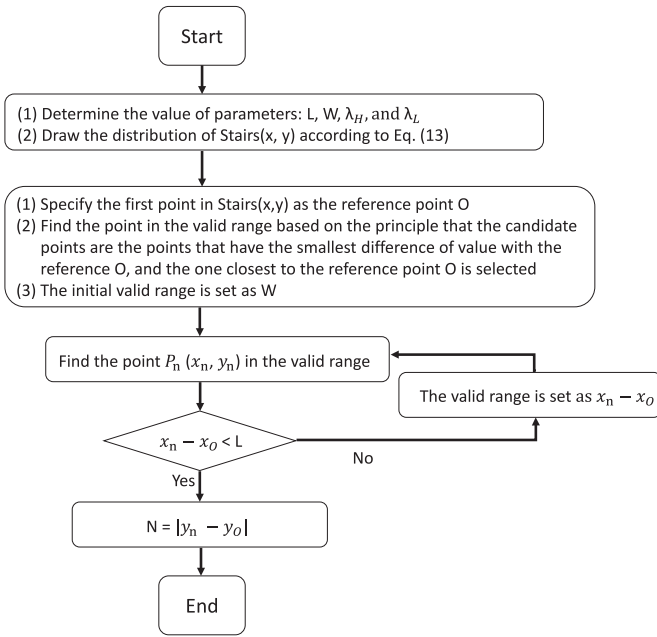
Fig. 3. The flowchart of the selection strategy.
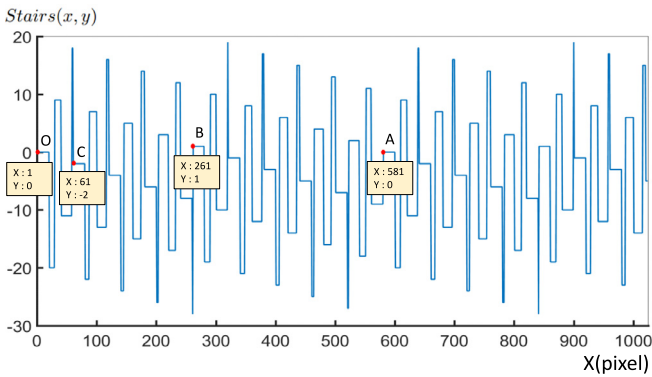
Fig. 4. The distribution of *Stairs*(*x*, *y*) for $\lambda_H = 20$ pixels and $\lambda_L = 29$ pixels.
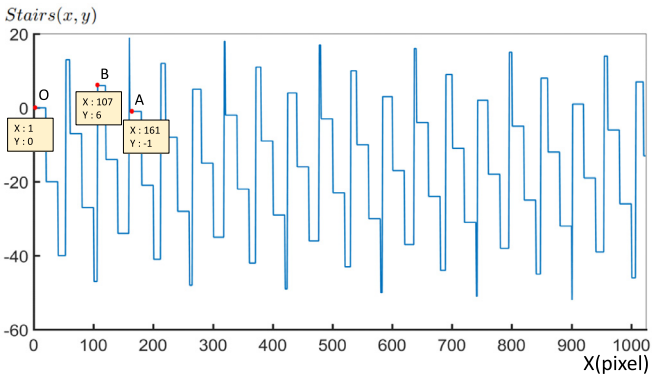
Fig. 5. The distribution of *Stairs*(*x*, *y*) for $\lambda_H = 20$ pixels and $\lambda_L = 53$ pixels.

Step 3 Judge the depth range, re-determine the target point (if applicable) and find *N*: Comparing the value of *L* and the distance between the target point and the reference point, the target point needs to be re-determined in the narrow range, defined by the reference point and the ex-target point, until the distance conforms to the given depth constraint. As shown in Fig. 4, the points
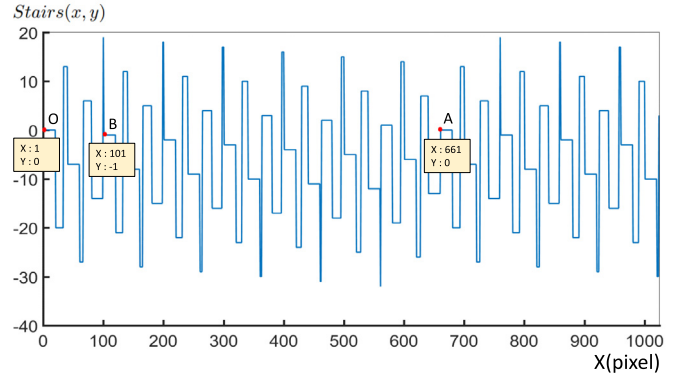
Fig. 6. The distribution of *Stairs*(*x*, *y*) for $\lambda_H = 20$ pixels and $\lambda_L = 33$ pixels.

A, B, C are selected in turn and *C* is re-determined as the final target point because the distances $x_A - x_O$ and $x_B - x_O$ all exceed *L* and $x_C - x_O$ is smaller than *L*, the limitation of depth constraint. Consequently, the value of *N* is 2 for the current parameters.

From the above description, the depth constraint *L* is 150 pixels, *W* is 1024 pixels, λ_H is 20 pixels, and λ_L is 29 pixels, so the minimum gap *N* is 2 in the unambiguous range (260 pixels, determined by $x_B - x_O$) as shown in Fig. 4. In the selection strategy, we reduce the unambiguous range until it is less than the depth constraint *L* to find the minimum gap *N*. It is obvious that the minimum gap *N* is larger within the smaller range. We gradually narrow the unambiguous range to get an optimal local range, which should be at least larger than *L* and provides a relatively large gap *N* (260 > *L* = 150). It should be pointed out that the proposed strategy of narrowing the unambiguous range step by step may not be the only way to determine *N*, but it is quite simple and straight-forward to obtain the accurate local unambiguous range. Based on the above process, we can optimize the wavelengths of the fringe patterns λ_L and λ_H so that the value of $\pi N/(p_L + p_H)$ can be maximized, resulting in optimal stability of phase unwrapping and robustness to noise.

Since the depth of focus of the camera and the slight defocusing range of the projector are limited in fact, the optimal depth range of measurement is fixed in a practical measurement system. So the depth constraint *L* can serve as a system constant. Considering that our method is adopted in high-speed measurement system where the binary defocusing patterns are not ideally sinusoidal and the exposure times of camera and projector are extremely limited, the captured image is of unideal contrast and is more susceptible to the noise. So it is necessary that the wavelengths of the fringe should be carefully selected. Due to the defocusing effect of the projector, λ_H, which determine the measurement accuracy of the system, is about 20 pixels, and a less-than-20-pixel wavelength cannot make obvious improvement of the precision in the binary defocusing fringe projection system. Together, the restrained defocusing level of the projector lens caused by hardware limitation will lead to the fact that a desired low-frequency fringe pattern cannot be generated. In conclusion, *L* is 150 pixels in our system, λ_H is set as 20 pixels which do not induce any phase errors for the four-step phase-shifting algorithm. The reasonable value of λ_L ranges from 21 to 60 pixels and λ_L is determined for it provides the highest accuracy of phase unwrapping after going through all the possible value. In this way, we can acquire the optimal bi-frequency scheme which maximizes the value of $\pi N/(p_L + p_H)$ and provides better accuracy for phase unwrapping. The selection strategy's further application is versatile with the adaption of the parameter mentioned above.

3. Simulations

To verify the performance of the proposed approach, we simulated the results of phase unwrapping under the different levels of noise. The

Table 1
The different bi-frequency schemes using different methods.

	The traditional approach	Our method (the optimal scheme)	Our method (the non-optimal scheme)
λ_H	20 pixels	20 pixels	20 pixels
λ_L	53 pixels	53 pixels	33 pixels
$LCM(\lambda_H, \lambda_L)$	1060 pixels	1060 pixels	660 pixels
The unambiguous range	1060 pixels	160 pixels	660 pixels
N	1	6	1
$\Delta\phi_{\max}$	$0.043\,rad$	$0.2582\,rad$	$0.0593\,rad$

different bi-frequency schemes using different experimental parameters shown in Table 1. The optimal scheme can provide larger $\Delta\phi_{\max}$, yet the non-optimal scheme only provides lower $\Delta\phi_{\max}$ due to the improper λ_L. In this simulation, L and W are set as 150 pixels and 1024 pixels. The unambiguous range in the traditional approach is 1060 pixels, which satisfies $1024 < LCM(\lambda_H, \lambda_L)$. The maximum phase noise tolerance $\Delta\phi_{max1}$ is 0.043 rad, which demonstrates that the conventional number-theoretical approach is sensitive to noise. Adopting the same wavelength in our method, as shown in Fig. 5, we found the minimum gap N_2 is 6 in the local range (160 pixels > L = 150 pixels) and the noise tolerance $\Delta\phi_{max2}$ is improved to 0.2582 rad. Also, we adjusted the value of λ_L to 33 pixels to test the proposed selection strategy, and found the final maximal phase error $\Delta\phi_{max3}$ is 0.0593 rad (see Fig. 6), which is slightly better than the conventional number-theoretical approach ($\Delta\phi_{max1} = 0.043\ rad$) but far inferior to the optimal wavelengths combination ($\Delta\phi_{max2} = 0.2582\ rad$).

Secondly, the simulation results are shown in Fig. 7. The error rate represents the ratio between the absolute phase of the fringes with and without noise. Fig. 7(a)–(c) show that the traditional approach cannot realize the global phase unwrapping under the different levels of noise since its inherent shortcoming. And without using the selection strategy of the optimal bi-frequency scheme, the additional bi-frequency scheme (λ_H = 20 pixels and λ_L = 33 pixels) is also failed to provide the sufficient stability to unwrap a high-frequency phase using our method as shown in Fig. 7(d)–(f). The simulation results proved that the optimal bi-frequency scheme (λ_H = 20 pixels and λ_L = 53 pixels) have the robust anti-noise capability using our method since it has a smaller error rate under the different levels of noise. In other words, we can realize phase unwrapping of higher frequency fringes compared to the traditional approach. Further, it also indicates that the selection strategy of the optimal bi-frequency scheme plays an important role to enhance the stability of the absolute phase recovery in our method.

4. Experimental results

A high-speed FPP system was set up to test the performance of the proposed method. This system includes a high-speed CMOS camera (Vision Research Phantom V611) and a high-speed DLP projection system as shown in Fig. 8. The high-speed projection system consists of a DLP development kit (Texas Instruments DLP Discovery 4100), an XGA resolution (1024 × 768) DMD, and a custom-designed optics module [29]. Based on the binary defocusing fringe projection technique, we drive the DMD at a refresh rate up to 20,000 binary fps [31]. The binary patterns with different fringes are generated by the binary dithering algorithm [53]. Since our approach uses 6 fringe patterns to recover one absolute phase map, the 3-D shape measurement speed is 3333 frames per second.

4.1. Scene I: experimental comparisons

Firstly, we experimentally verified the simulation results by measuring a plaster model using the same fringe patterns as shown in Fig. 9. The absolute phase maps of the tested object were calculated using different approaches as shown in Fig. 9(b), (e), and (h). In addition, the absolute

phase map obtained using the 12-step phase-shifting method based on multi-frequency temporal phase unwrapping approach can serve as the ground truth, and the phase difference maps are provided in Fig. 9(c), (f), and (i), in which the proposed method with fringe patterns (λ_H = 20 pixels and λ_L = 53 pixels) contains fewer phase errors compared with others. Fig. 9(c) and (f) are able to prove that the proposed method (using depth constraint) provides better reliability of phase unwrapping, while the traditional number-theoretical TPU approach is more susceptible to noise. In general, the binary dithering algorithm cannot generate a desired fringe pattern when the fringe is very wide. The low-quality fringe is unsuitable to the traditional number-theoretical TPU approach, whose phase error exceeds the threshold of the traditional maximal phase error. However, this fringe can be applied to correctly unwrap the wrapped phase computed from high-frequency fringes using our method. Fig. 9(f) and (i) show that the results are similar to our simulation results. The nose of the tested plaster model is in the low signal-to-noise ratio (SNR) region which can be used to test the reliability of phase unwrapping under noisy condition. The experimental results show that λ_H = 20 pixels and λ_L = 53 pixels can provide better reliability of phase unwrapping compared to λ_H = 20 pixels and λ_L = 33 pixels. The experimental results suggest that the wavelength of the bi-frequency scheme (λ_H, λ_L) should be carefully selected to make phase unwrapping more reliable. Notably, this result demonstrates once again that the selection strategy can be used to provide the optimal bi-frequency scheme for our system, which can improve the stability of the absolute phase recovery.

4.2. Scene II: Accuracy analysis

To quantitatively compare 3-D measurement precision of the traditional approach and our method, we measured a standard ceramic sphere with radius R = 25.4 mm. In our method, the optimal bi-frequency scheme (λ_H = 20 pixels and λ_L = 53 pixels) were further used in this experiment to achieve higher precision 3-D reconstruction results. In the traditional number-theoretical approach, for acquiring the similar stability to unwrap the wrapped phase, the fringe pitch of the bi-frequency scheme was set as λ_H = 40 pixels and λ_L = 47 pixels to realize phase unwrapping in global range. The measurement results are shown in Fig. 10. Fig. 10(a) and (d) display the 3-D reconstruction results using different methods. After the 3-D data of the sphere surface was obtained, we fitted it to the standard sphere whose point cloud represents the spherical surface. The differences between the measured data and the fitted sphere represent the measurement errors as shown in Fig. 10(b) and (e). And the quantitative histograms of the differences are shown in Fig. 10(c) and (f). It can be easily found that the RMS of the measured errors are 96.237 μm and 53.664 μm, respectively. Compared with the traditional number-theoretical approach, our method can significantly increase the measurement accuracy due to the use of high-frequency fringe patterns and high SNR of the recovered phase map.

4.3. Scene III: static and dynamic scenes measurement

After confirming 3-D measurement precision of our system, the optimal bi-frequency scheme is widely used to obtain 3-D reconstruction
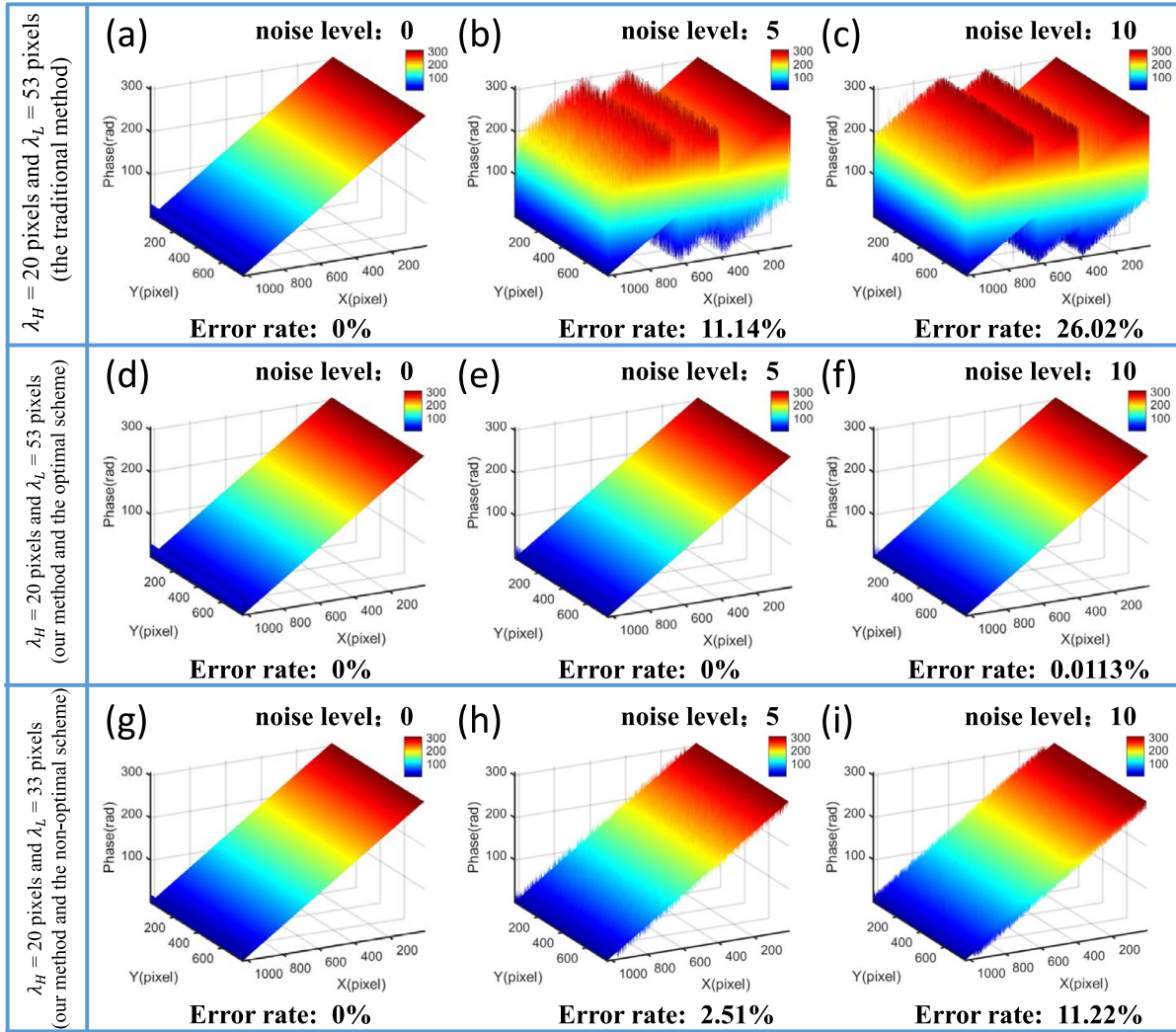
Fig. 7. The simulation results of phase unwrapping under the different levels of noise.

Fig. 8. This system includes a high-speed CMOS camera and a DLP projection system.

results in this subsection. It is worthwhile to note that the optimal bi-frequency scheme can acquire 3-D information of an object in a depth range of 200 mm. The further experiments were carried out to verify the stability of our system for multiples objects with complex shapes. A number of different objects were measured including the statue of David, a triangular cone model, a plaster geometric model, and a cartoon face. The 3-D results obtained by our method are shown in Fig. 11. The ex-

perimental results demonstrate the capability of the proposed method to achieve robust 3-D shape measurement for objects with complex surfaces and geometric discontinuities.

Next, our system is applied to high-speed 3-D shape measurement of a dynamic object: a free-falling balloon filled with water. Fig. 12 show representative 2D camera images (one of the four-step phase-shifting patterns) and corresponding color-coded 3-D reconstructions at different time points. The balloon is artificially suspended in the air and remains stationary until it is released (T = 25 ms). After traveling in free fall for about 125 ms, the balloon arrives and began to be deformed by the ground. Then, the balloon has undergone severe deformation, losing its original smooth shape (T = 175 ms). Due to the ground reaction force, the balloon gradually returns to its former appearance (T = 210 ms). Moreover, the balloon bounces back into the air again (T = 315 ms). After several repeated bounces, the balloon finally falls back to the ground (T = 885 ms). The whole 3-D measurement results can be referred to in Visualization 1. During the whole process, the surface of the balloon was correctly reconstructed with high-quality, demonstrating the reliability of the proposed method to perform high-precision absolute 3-D shape measurement.

In the last measurement, we applied our system to imaging one-time transient event: a bullet fired from a toy gun and then rebounded from a plastic plate. Fig. 13(a) and (b) show representative camera images (one of the four-step phase-shifting patterns) and corresponding color-coded
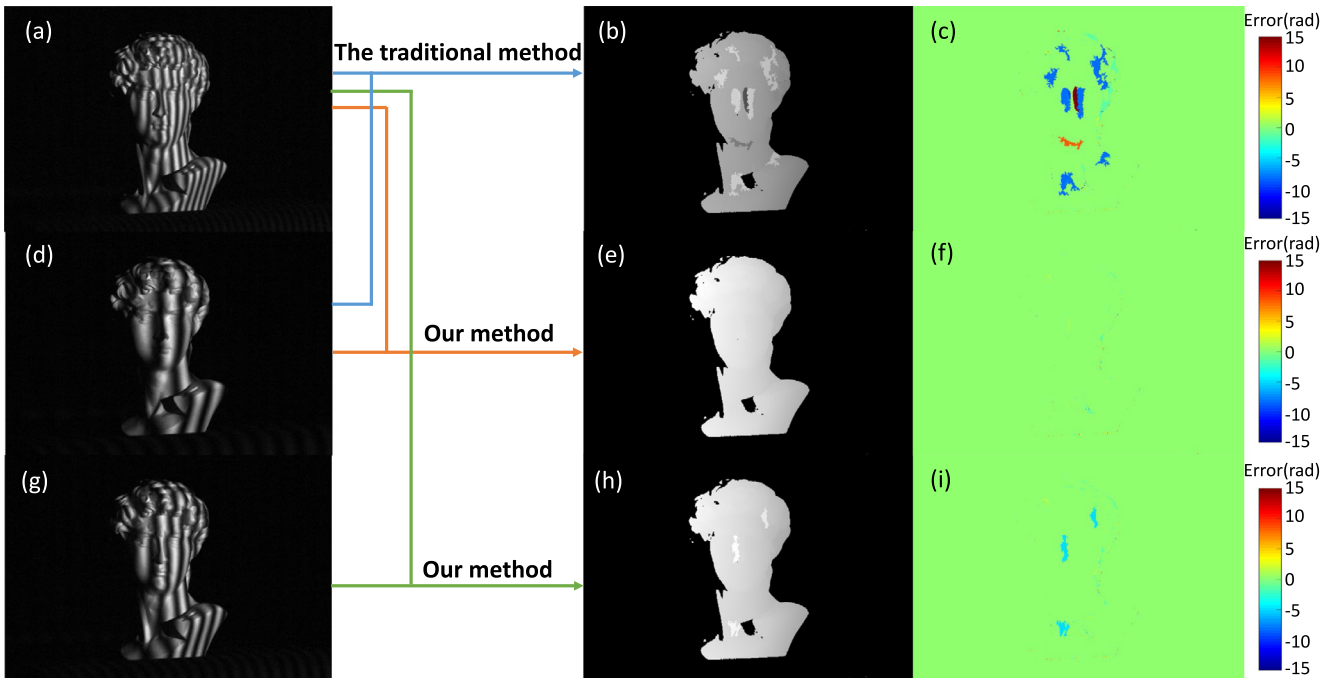
Fig. 9. (a) The captured scene with fringe patterns (λ_H = 20 pixels). (b) The absolute phase map by using the traditional number-theoretical approach with fringe patterns (λ_H = 20 pixels and λ_L = 53 pixels). (c) The phase difference map between (b) and the ground truth. (d) The captured scene with fringe patterns (λ_L = 53 pixels). (e) The absolute phase map by using the proposed method with fringe patterns (λ_H = 20 pixels and λ_L = 53 pixels). (f) The phase difference map between (e) and the ground truth. (g) The captured scene with fringe patterns (λ_L = 33 pixels). (h) The absolute phase map by using the proposed method with fringe patterns (λ_H = 20 pixels and λ_L = 33 pixels). (i) The phase difference map between (h) and the ground truth.
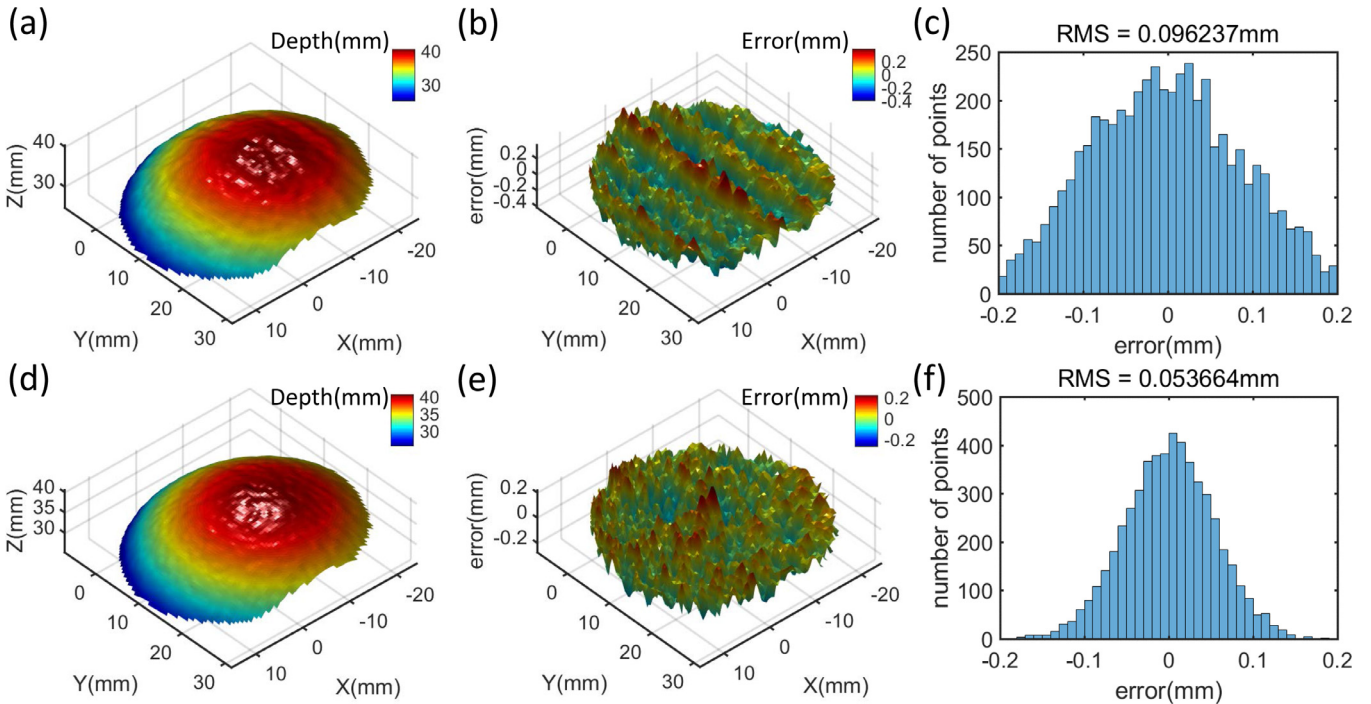
Fig. 10. Precision analysis for a standard ceramic spheres. (a) 3-D reconstruction result using the traditional number-theoretical approach. (b) The distribution of the errors of (a). (c) The histogram of (b). (d) 3-D reconstruction result using our method. (e) The distribution of the errors of (d). (f) The histogram of (e).

3-D reconstructions at different time points. T = 0 ms was the start of the observation time, and the bullet was fired from the gun muzzle at about T = 17.5 ms. After traveling in free-flight for about 23 ms, the bullet hit the plate and rebounded towards the gun. During the later 110 ms, the plate was back and forth as a result of the inertia. In Fig 13(c),

we show the 3-D reconstruction of the bullet at five different points of time (17.5 ms, 29 ms, 40 ms, 75 ms, and 153 ms). The 3-D data can be used to quantitatively analyze the process with regards to the ballistic trajectory and velocity. In Fig 13(d), we show the reconstructed 3-D shapes of the plate at three different time points (0 ms, 75 ms, and
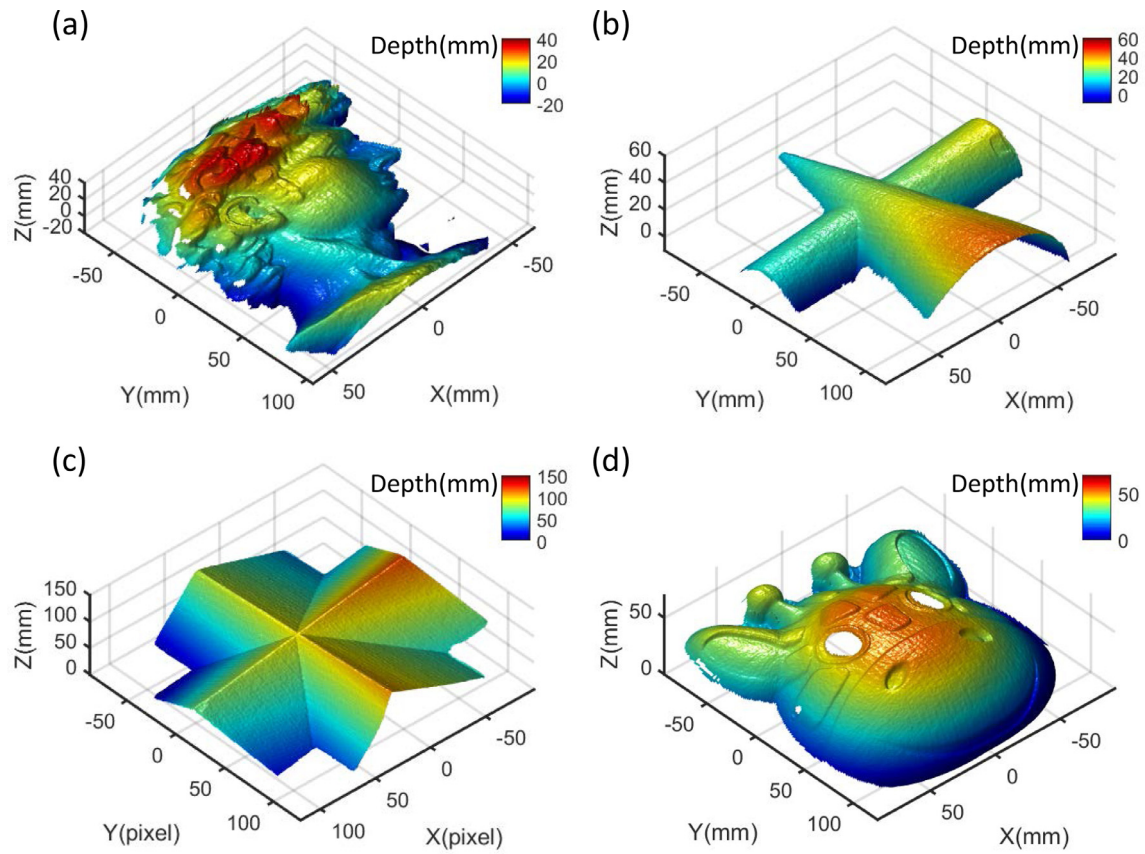
Fig. 11. Measurement results of several objects. (a) The statue of David. (b) A triangular cone model. (c) A plaster geometric model. (d) A cartoon face.
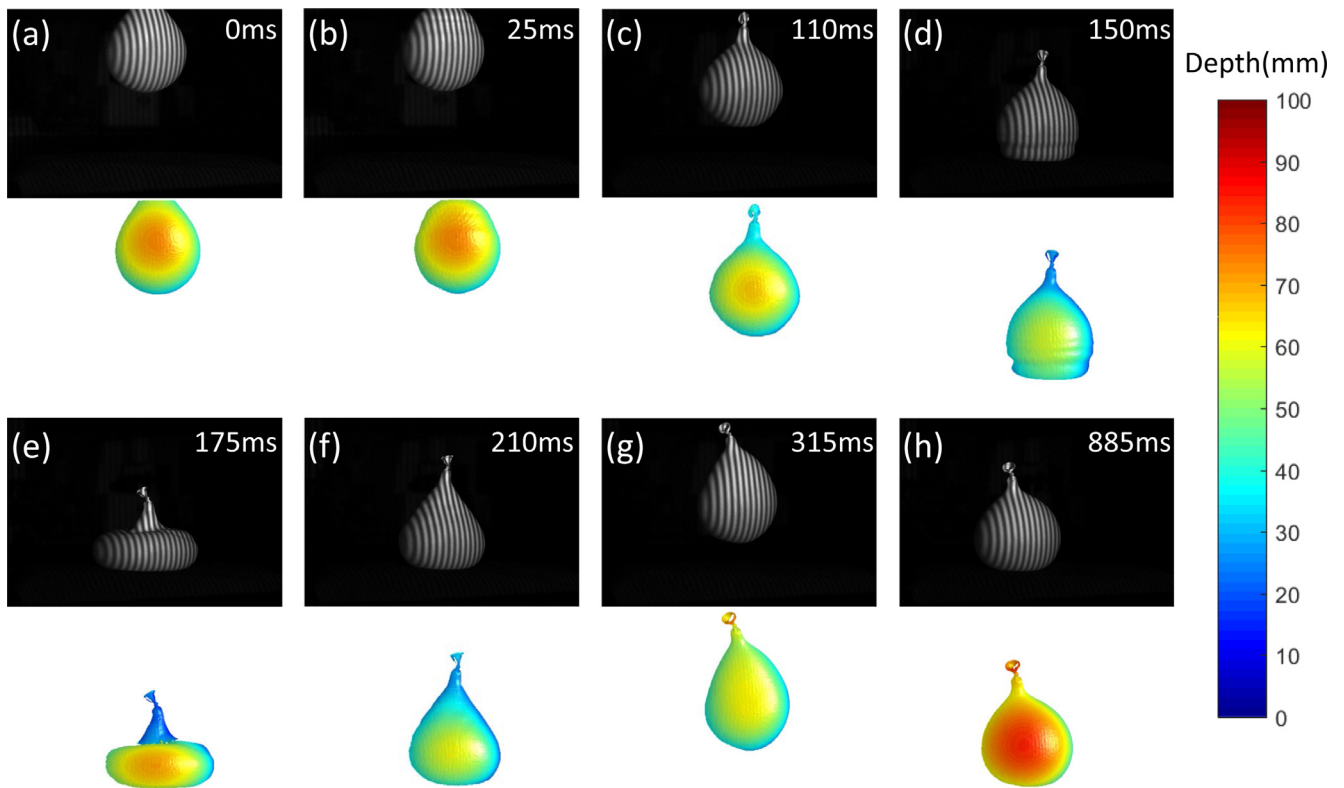
Fig. 12. A balloon filled with water falls freely. (a)–(h) show 2D camera images (one of the four-step phase-shifting patterns) and corresponding color-coded 3-D reconstructions at the time points of 0 ms, 25 ms, 110 ms, 150 ms, 175 ms, 210 ms, 315 ms, and 885 ms. (For interpretation of the references to color in this figure legend, the reader is referred to the web version of this article.)
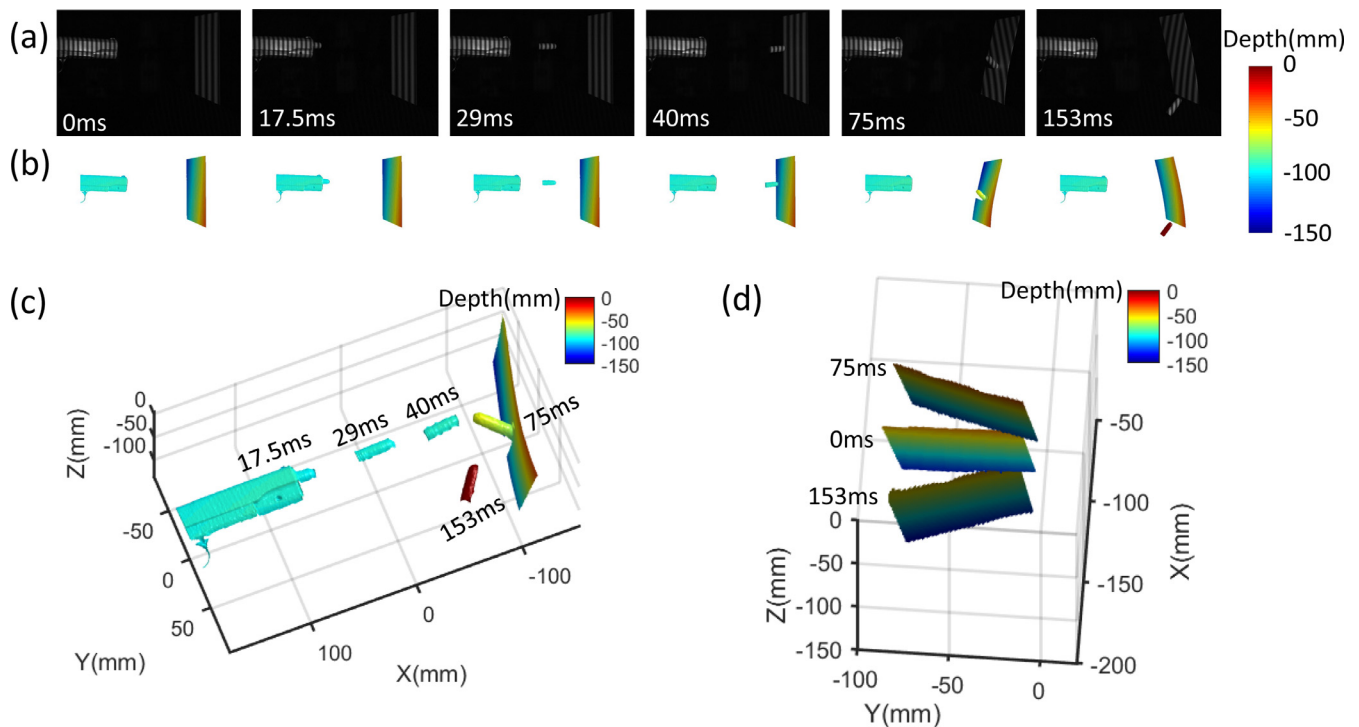
Fig. 13. A bullet fired from a toy gun and then rebounded from a plastic plate. (a)-(b) show 2D camera images (one of the four-step phase-shifting patterns) and corresponding color-coded 3-D reconstructions at different times. (c) shows the 3-D reconstruction of the bullet at 17.5 ms, 29 ms, 40 ms, 75 ms, and 153 ms. (d) shows the reconstructed 3-D shapes of the plate at 0 ms, 75 ms, and 153 ms. (For interpretation of the references to color in this figure legend, the reader is referred to the web version of this article.)

153 ms). A more detailed illustration of the transient event is provided in Visualization 2, which is a slow-motion 3-D movie containing 4000 3-D frames (corresponding to an observation period of 200 *ms*). This experiment successfully demonstrated that our proposed method can measure multiple isolated objects at high speed.

5. Conclusions

In this work, a novel high-speed 3-D shape measurement technique for dynamic scenes using geometry-constraint-based number-theoretical TPU has been presented. By introducing depth constraint into the traditional number-theoretical TPU, the unambiguous phase range can be reduced from the conventional global range of the projector coordinate to a smaller period range defined by the depth range. Due to the reduction of fringe order candidates and the unambiguous phase range, the reliability of phase unwrapping can be significantly improved compared with the traditional number-theoretical TPU approach even when high-frequency fringe patterns are used. Benefitting from the number-theoretical approach based on depth constraint, a global absolute phase map of high-frequency, dense fringes can be unwrapped using binary dithering patterns. Furthermore, a simple and effective selection strategy of the optimal bi-frequency scheme has been proposed to provide better reliability of phase unwrapping. We have demonstrated that with the proposed scheme, the phase unwrapping error due to dithering and random noise can be substantially reduced. 3-D shape measurement results at 3333 frames per second have also demonstrated its potential for high-speed, high-precision, non-ambiguity, and full-field 3-D data acquisition and analysis, rendering it a promising technique of dynamic 3-D shape measurement for complex surfaces and spatially isolated objects.

Acknowledgments

Supplementary material

Supplementary material associated with this article can be found, in the online version, at doi:10.1016/j.optlaseng.2018.11.006

References

[1] Gorthi SS, Rastogi P. Fringe projection techniques: whither we are? Opt Lasers Eng 2010;48(IMAC-REVIEW-2009-001):133–40.

[2] Su X, Zhang Q. Dynamic 3-d shape measurement method: a review. Opt Lasers Eng 2010;48(2):191–204.

[3] Van der Jeught S, Dirckx JJ. Real-time structured light profilometry: a review. Opt Lasers Eng 2016;87:18–31.

[4] Zhang S. Recent progresses on real-time 3d shape measurement using digital fringe projection techniques. Opt Lasers Eng 2010;48(2):149–58.

[5] Zhang S. High-speed 3d shape measurement with structured light methods: a review. Opt Lasers Eng 2018;106:119–31.

[6] Zhang Z. Review of single-shot 3d shape measurement by phase calculation-based fringe projection techniques. Opt Lasers Eng 2012;50(8):1097–106.

[7] Srinivasan V, Liu HC, Halioua M. Automated phase-measuring profilometry of 3d diffuse objects. Appl Opt 1984;23(18):3105–8.

[8] Zuo C, Feng S, Huang L, Tao T, Yin W, Chen Q. Phase shifting algorithms for fringe projection profilometry: a review. Opt Lasers Eng 2018;109:23–59.

[9] Su X, Chen W. Fourier transform profilometry: a review. Opt Lasers Eng 2001;35(5):263–84.

[10] Takeda M, Mutoh K. Fourier transform profilometry for the automatic measurement of 3-d object shapes. Appl Opt 1983;22(24):3977–82.

[11] Kemao Q. Windowed fourier transform for fringe pattern analysis. Appl Opt 2004;43(13):2695–702.

[12] Zhong J, Weng J. Spatial carrier-fringe pattern analysis by means of wavelet transform: wavelet transform profilometry. Appl Opt 2004;43(26):4993–8.

[13] Su X, Chen W. Reliability-guided phase unwrapping algorithm: a review. Opt Lasers Eng 2004;42(3):245–61.

[14] Zuo C, Huang L, Zhang M, Chen Q, Asundi A. Temporal phase unwrapping algorithms for fringe projection profilometry: a comparative review. Opt Lasers Eng 2016;85:84–103.

[15] Sansoni G, Carocci M, Rodella R. Three-dimensional vision based on a combination of gray-code and phase-shift light projection: analysis and compensation of the systematic errors. Appl Opt 1999;38(31):6565–73.

[16] Wang Y, Zhang S. Novel phase-coding method for absolute phase retrieval. Opt Lett 2012;37(11):2067–9.

[17] Hyun J-S, Zhang S. Superfast 3d absolute shape measurement using five binary patterns. Opt Lasers Eng 2017;90:217–24.

[18] Goldstein RM, Zebker HA, Werner CL. Satellite radar interferometry: two-dimensional phase unwrapping. Radio Sci 1988;23(4):713–20.

[19] Flynn TJ. Two-dimensional phase unwrapping with minimum weighted discontinuity. JOSA A 1997;14(10):2692–701.

[20] Ghiglia DC, Romero LA. Minimum lp-norm two-dimensional phase unwrapping. JOSA A 1996;13(10):1999–2013.

[21] Zhao M, Huang L, Zhang Q, Su X, Asundi A, Kemao Q. Quality-guided phase unwrapping technique: comparison of quality maps and guiding strategies. Appl Opt 2011;50(33):6214–24.

[22] Zuo C, Chen Q, Gu G, Feng S, Feng F, Li R, et al. High-speed three-dimensional shape measurement for dynamic scenes using bi-frequency tripolar pulse-width-modulation fringe projection. Opt Lasers Eng 2013;51(8):953–60.

[23] Tao T, Chen Q, Da J, Feng S, Hu Y, Zuo C. Real-time 3-d shape measurement with composite phase-shifting fringes and multi-view system. Opt Express 2016;24(18):20253–69.

[24] Zhang Q, Su X. High-speed optical measurement for the drumhead vibration. Opt Express 2005;13(8):3110–16.

[25] Zhang S, Van Der Weide D, Oliver J. Superfast phase-shifting method for 3-d shape measurement. Opt Express 2010;18(9):9684–9.

[26] Xu Y, Chen C, Huang S, Zhang Z. Simultaneously measuring 3d shape and colour texture of moving objects using ir and colour fringe projection techniques. Opt Lasers Eng 2014;61:1–7.

[27] Tao T, Chen Q, Feng S, Hu Y, Da J, Zuo C. High-precision real-time 3d shape measurement using a bi-frequency scheme and multi-view system. Appl Opt 2017;56(13):3646–53.

[28] Hu Y, Chen Q, Feng S, Tao T, Li H, Zuo C. Real-time microscopic 3-d shape measurement based on optimized pulse-width-modulation binary fringe projection. Meas Sci Technol 2017;28(7):075010.

[29] Zuo C, Tao T, Feng S, Huang L, Asundi A, Chen Q. Micro fourier transform profilometry (μftp): 3d shape measurement at 10,000 frames per second. Opt Lasers Eng 2018;102:70–91.

[30] Feng S, Zuo C, Tao T, Hu Y, Zhang M, Chen Q, et al. Robust dynamic 3-d measurements with motion-compensated phase-shifting profilometry. Opt Lasers Eng 2018;103:127–38.

[31] Lei S, Zhang S. Flexible 3-d shape measurement using projector defocusing. Opt Lett 2009;34(20):3080–2.

[32] Ekstrand L, Zhang S. Three-dimensional profilometry with nearly focused binary phase-shifting algorithms. Opt Lett 2011;36(23):4518–20.

[33] Wang Y, Zhang S. Three-dimensional shape measurement with binary dithered patterns. Appl Opt 2012;51(27):6631–6.

[34] Cheng YY, Wyant JC. Two-wavelength phase shifting interferometry. Appl Opt 1984;23(24):4539–43.

[35] Creath K, Cheng YY, Wyant JC. Contouring aspheric surfaces using two-wavelength phase-shifting interferometry. Optica Acta: International Journal of Optics 1985;32(12):1455–64.

[36] Towers CE, Towers DP, Jones JD. Optimum frequency selection in multifrequency interferometry. Opt Lett 2003;28(11):887–9.

[37] Gushov V, Solodkin YN. Automatic processing of fringe patterns in integer interferometers. Opt Lasers Eng 1991;14(4–5):311–24.

[38] Ding Y, Xi J, Yu Y, Chicharo J. Recovering the absolute phase maps of two fringe patterns with selected frequencies. Opt Lett 2011;36(13):2518–20.

[39] Ding Y, Xi J, Yu Y, Cheng W, Wang S, Chicharo JF. Frequency selection in absolute phase maps recovery with two frequency projection fringes. Opt Express 2012;20(12):13238–51.

[40] Zhong J, Zhang Y. Absolute phase-measurement technique based on number theory in multifrequency grating projection profilometry. Appl Opt 2001;40(4):492–500.

[41] Zhang Z. Determining the epipolar geometry and its uncertainty: a review. Int J Comput Vis 1998;27(2):161–95.

[42] Liu X, Kofman J. High-frequency background modulation fringe patterns based on a fringe-wavelength geometry-constraint model for 3d surface-shape measurement. Opt Express 2017;25(14):16618–28.

[43] Zhong K, Li Z, Shi Y, Wang C, Lei Y. Fast phase measurement profilometry for arbitrary shape objects without phase unwrapping. Opt Lasers Eng 2013;51(11):1213–22.

[44] Li Z, Zhong K, Li YF, Zhou X, Shi Y. Multiview phase shifting: a full-resolution and high-speed 3d measurement framework for arbitrary shape dynamic objects. Opt Lett 2013;38(9):1389–91.

[45] An Y, Hyun J-S, Zhang S. Pixel-wise absolute phase unwrapping using geometric constraints of structured light system. Opt Express 2016;24(16):18445–59.

[46] Tao T, Chen Q, Feng S, Hu Y, Zhang M, Zuo C. High-precision real-time 3d shape measurement based on a quad-camera system. J Opt 2017;20(1):014009.

[47] Liu X, Kofman J. Background and amplitude encoded fringe patterns for 3d surface-shape measurement. Opt Lasers Eng 2017;94:63–9.

[48] Hyun J-S, Zhang S. Enhanced two-frequency phase-shifting method. Appl Opt 2016;55(16):4395–401.

[49] Li J, Hassebrook LG, Guan C. Optimized two-frequency phase-measuring-profilometry light-sensor temporal-noise sensitivity. JOSA A 2003;20(1):106–15.

[50] Feng S, Zhang Y, Chen Q, Zuo C, Li R, Shen G. General solution for high dynamic range three-dimensional shape measurement using the fringe projection technique. Opt Lasers Eng 2014;59:56–71.

[51] Su X-Y, Von Bally G, Vukicevic D. Phase-stepping grating profilometry: utilization of intensity modulation analysis in complex objects evaluation. Opt Commun 1993;98(1–3):141–50.

[52] Liu K, Wang Y, Lau DL, Hao Q, Hassebrook LG. Dual-frequency pattern scheme for high-speed 3-d shape measurement. Opt Express 2010;18(5):5229–44.

[53] Lohry W, Zhang S. Genetic method to optimize binary dithering technique for high-quality fringe generation. Opt Lett 2013;38(4):540–2.